REPORT DOCUMENTATION PAGE

Form Approved
OMB No. 0704-0188

1. AGENCY USE ONLY (Leave Blank)	2. REPORT DATE	3. REPORT TYPE AND DATES COVERED
	March 15, 1999	**Final Report, August 19, 1998 to February 18, 1999**

4. TITLE AND SUBTITLE

REAL-TIME, TWO-DIMENTIONAL TERAHERTZ BEAM IMAGING

5. FUNDING NUMBERS

DAAG55-98-C-0071

6. AUTHOR(S)

Xi-Cheng Zhang and Zhiping Jiang

7. PERFORMING ORGANIZATION NAME (S) AND ADDRESS(ES)

Zomega Technology Corp.
31 Omega Terrace, Latham, NY 12110

8. PERFORMING ORGANIZATION REPORT NUMBER

F-3-1999

9. SPONSORING/MONITORING AGENCY NAME(S) AND ADDRESS(ES)

Army Research Office
P.O. Box 12211
Research Triangle Park, NC 27709-2211

10. SPONSORING/MONITORING AGENCY REPORT NUMBER

11. SUPPLEMENTARY NOTES

12a. DISTRIBUTION/AVAILABILITY STATEMENT

Approved for public release; distribution unlimited.

12b. DISTRIBUTION CODE

13. ABSTRACT (Maximum 200 words)

Report developed under STTR contract DAAG55-98-C-0071.

In ARO STTR Phase I program, we have demonstrated the concept and developed a real-time, two-dimensional THz wave imaging system. The THz imaging system uses electro-optic crystals and is capable of time-domain far-infrared spectroscopy across a frequency range extending from near DC to several THz. We have improved THz imaging spatial resolution by one order.

We have designed and started to construct a portable THz beam system for commercial applications. In particular, we have demonstrated the feasibility of using a chirped optical probe pulse to read THz imaging in an electro-optic crystal which provides the measurement of a THz wave with an unprecedented data acquisition rate.

We have attracted over $30,000 outside funding for THz research and commercialization. We have established a network with scientists and researchers in THz field.

14. SUBJECT TERMS

STTR Phase I Final Technical Report

15. NUMBER OF PAGES

20

16. PRICE CODE

17. SECURITY CLASSIFICATION OF REPORT	18. SECURITY CLASSIFICATION OF THIS PAGE	19. SECURITY CLASSIFICATION OF ABSTRACT	20. LIMITATION OF ABSTRACT
			UL

ZOmega Technology Corp.
31 Omega Terrace, Latham, NY, 12110
Tel/Fax: (518) 786-1684/6450

TABLE OF CONTENTS

ZOmega Technology Corp.
31 Omega Terrace, Latham, NY, 12110
Tel/Fax: (518) 786-1684/6450

Real-Time, Two-Dimensional Terahertz Wave Imaging

(Final Technical Report: ARO-STTR, DAAG55-98-C-0071)

In this ARO-STTR Phase I program, we completed the proof-of-principle analysis of real-time, two-dimensional terahertz (THz) wave imaging, including theoretical modeling to select optimal components such as the THz emitter, the electro-optic crystal, the CCD, and optical design. We demonstrated the feasibility for building a real-time, two-dimensional, terahertz wave imaging system with a resolution exceeding 100x100 pixels at video frame rates. We have started to build the 4th prototype THz system.

Our achievements in this STTR phase I program include:

(1) THz field measurement in liquid

The THz Imaging Laboratory at Rensselaer Polytechnic Institute demonstrated the use of liquid to measure free-space electromagnetic pulses. One of the most important results is that we can measure the EM field in the water. Water is of major importance to all living things; in some organisms, up to 90 percent of their body weight comes from water. Up to 60 percent of the human body is water, the brain is composed of 70 percent water, blood is 82 percent water, and the lungs are nearly 90 percent water. Based on our demonstration we believe that we may be able to measure the EM field strength in a living body by using the light. We realized that possible impact: this work may provide an alternative method for the study of the human body damage by using a high frequency cellular phone (EM radiation) and the effect of high voltage power line in the home backyard.

It is possible to use liquids to measure free-space THz pulses via the Faraday effect. We demonstrate the use of water, tea, Pepsi®, and many other polar and non-polar liquids as electromagnetic sensors. In general, liquids are not electro-optically active, so the electro-optic effect, which only occurs at the surface or interface, is extremely weak. However, since most liquids have a non-zero Verdet constant, magneto-optic measurement through the Faraday effect is plausible for the measurement of a THz pulse. Unlike direct measurement of the electric component of the THz electromagnetic pulse by the Pockels effect, the magneto-optic Faraday effect directly senses the magnetic component.

(2) Zero optical based point in electro-optic imaging

Free space electro-optic detection demonstrated unique capability of parallel measurement for both spatial and temporal THz imaging. With the use of a CCD camera and a chirped optical probe pulse, real-time and single-shot images of THz field have been achieved. However, Due to the limited dynamic range of most CCD cameras (<18 bit) and the lack of multi-channel lock-in amplifier, to image a weak THz modulated optical signal carried on a large laser background, it has to work at a near-zero optical bias point to reduce the intense background light. One basic concern of this electro-optic measurement near the zero optical bias point is the optimal modulation depth, signal-to-noise ratio and the field quadratic dependence.

We solved the technical bottleneck problem for the THz imaging of a very weak signal. For example, we performed the theoretical analysis and experimental result of electro-optic sampling near the zero optical bias point. We showed that there is an optimal position in a crossed polarizer electro-optic geometry. At this point, free-space electro-optic sampling with a ZnTe crystal has the largest modulation depth for the detection of a weak THz modulated signal carried on a strong laser background. We also demonstrate that at this optimal position, the signal-to-noise ratio has the local maximum. We have achieved the experimental procedure to obtain this optimal working point.

We performed the theoretical and experimental study of electro-optic sampling near the zero optical bias point with a finite scattering light and the residue birefringence. It is found that both the scattered light and the residue birefringence reduce the extinction ratio, but usually the later is dominant. When the residue birefringence is compensated, the scattering light is the ultimate factor limiting the extinction ratio. Specifically we demonstrated that there is an optimal position which provides the largest modulation depth (as well as the signal-to-noise ratio) for the detection of a weak THz modulated signal carried on a strong laser background. During the experiment, only ZnTe sensors were used, however the concept could be generalized to other electro-optic crystals.

This achievement is crucial for our next step toward to optimal condition for THz imaging by providing better signal-to-noise ration and faster data acquisition time.

(3) Balanced electro-optic measurement

After we demonstrated that there is an optimal position which provides the largest modulation depth (as well as the signal-to-noise ratio) for the detection of a weak THz modulated signal carried on a strong laser background. We have found this optimal point by experimental demonstration and theoretical analysis. We also add a second attenuated probe beam which does not pass the ZnTe crystal onto a pair of the balanced photo-detectors to reduce noise. This achievement is crucial for our next step toward to optimal condition for THz imaging by providing better signal-to-noise ration and faster data acquisition time. We have applied this new method developed to detect a weak THz modulated signal carried on a strong laser background.

As one of the examples, Figure 1 schematically illustrates a THz imaging setup used to demonstrate this new method. The polarization of the polarizers was set in near cross geometry. A THz beam reads the object under test. This imaging system measures the small different in dielectric constant (both real and imaginary parts). For example, it provides spatial information of the THz transmission and length of the optical beam path through the samples.

The THz absorption less than 1% and a time delay less than 60 fs can be measured by our THz system. Figure 2 shows the THz image of the watermarks from several currencies. Clear images of these watermarks in THz spectrum show an alternative method for anti-counterfeiting.

ZOmega Technology Corp.
31 Omega Terrace, Latham, NY, 12110
Tel/Fax: (518) 786-1684/6450

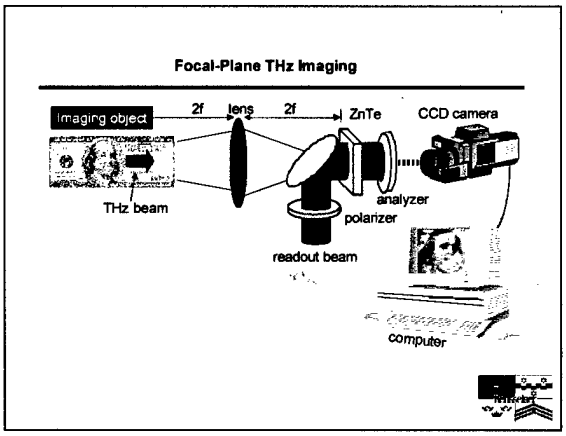

Fig. 1. Experimental setup

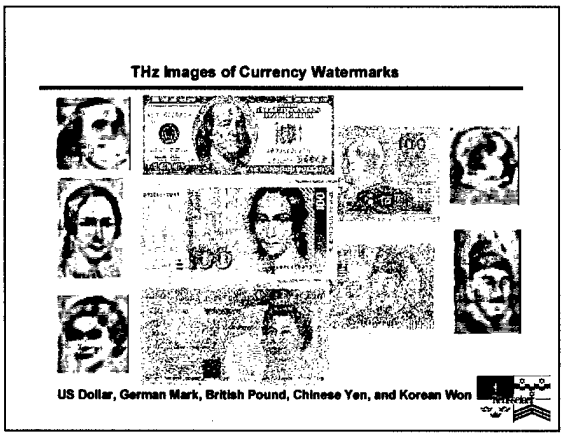

Fig. 2: THz images of watermarks

(4) Polarization Modulation

We have applied the polarization modulation technique for optoelectronic generation and detection of a THz beam. Compared to the conventional amplitude modulation with a lock-in amplifier, the optical polarization modulation provides a two-fold increase of the dynamic range. We will file a patent application for this invention.

The laser (Ti:sapphire oscillator and regenerative amplifier) produces a 250-fs pulse duration at 800 nm with a repetition rate of 250 kHz and an average power of 600mW. The pump optical beam (500mW) passing through an electro-optic modulator is focused onto a 2-mm thick <110> ZnTe to generate THz beam. In the conventional phase sensitive detection system with the amplitude modulation of the laser pump beam (even duty cycle) 50% of the laser power is blocked by the optical chopper, therefore half of the laser energy is wasted.

It is possible to fully utilize the total laser power by using the polarization modulation. An electro-optic modulator alternatively changes the polarization plane of a linear polarized laser beam at the modulation frequency. The ZnTe rectified crystal was set so as to radiate a positive THz signal at one polarization and a negative signal at the second polarization. This is because the sign and amplitude of the THz signal generated from the electro-optic crystal depend on the polarization of the incident optical beam. For example, for a <110> ZnTe rectified crystal, one polarization of the laser excitation beam (P_+) should be parallel to <1, -1,1> axis, and the second polarization P. should have an angle of about 70 degrees from P_+. In this case, the periodic polarization modulation of the laser pump beam generates the periodic THz beam with equal amplitude but an opposite sign. Once a lock-in amplifier is used, the total signal increases by a factor of 2, compared with the conventional "on/off" amplitude modulation method.

Compared with the conventional amplitude modulation with a lock-in amplifier, the optical polarization modulation in optoelectronic generation and detection of a free-space THz radiation provides a two-fold increase of the dynamic range.

Figure 3 plots the calculated peak amplitude of an optical rectified THz signal from a <110> zincblende crystal versus the polarization angle of the pump beam. The polarization of the optical excitation beam is modulated at linear polarization planes P_+ and P.. The angle ΔP between two polarization planes P_+ and P. is about 71 degrees.

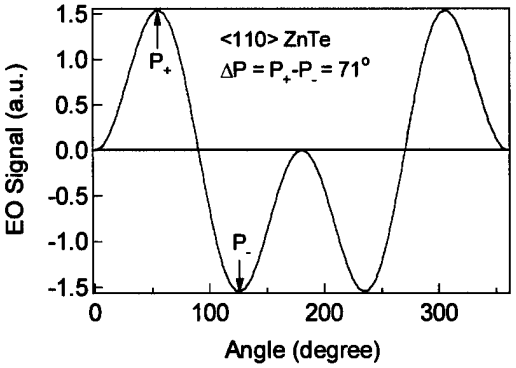

Fig. 3. Operation points for polarization modulation. The polarization planes of linearly polarized light are modulated at P_+ and P. at the modulation frequency.

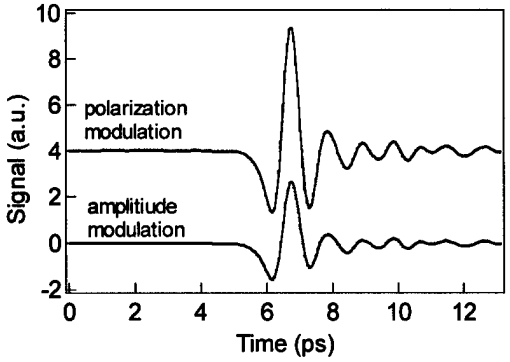

Fig. 4. Measured temporal waveforms by using polarization modulation and amplitude modulation.

Figure 4 shows the temporal THz waveforms obtained by using a mechanical chopper and by the polarization modulation technique, respectively. An external function generator drove the modulators with a square wave at the same frequency (1.87 kHz). The THz signal measured by using the polarization modulation is nearly twice the THz signal measured by using the mechanical chopper. This method applies to any polarization sensitive THz emitter.

(5) Mid-IR THz Imaging

We concentrated on the improvement of the spatial-temporal resolution. Due to the strong molecular resonance in the IR frequency region, a strong absorption is expected for the THz radiation in chemical and biological material. Thus a molecular-specific contrast of a structural form in this material is feasible by using a THz radiation source. The imaging of some samples in this category has been demonstrated by using far-IR THz pulses.

In contrast to cw technique, this time-domain technique provides us with an additional phase information. From the waveform not only the attenuation or absorption but also a dispersive property of the sample can be extracted. The ranging, e.g., a tomographic depth profile, is another convincing example for the superiority of the time-domain technique. More recently the free-space EO technique is used for two dimensional frame imaging of THz field distribution, showing a possibility toward a real-time single-short image.

A drawback of the far-IR imaging technique for a sub-millimeter imaging, however, is the inherent limitation of the spatial resolution. One way to increase the spatial

resolution is to use the concept of the near-field optics. This concept, however, limits the distance between the radiation source and the sample within an extremely shallow focal depth.

The transillumination of the waveform is recorded, while the sample is scanned laterally using two motorized translation stages. A two-dimensional contrast image is achieved by plotting the transillumation amplitude of the THz waveform at a fixed time-delay between the excitation and the probe pulse. Even most our standard THz imaging are capable for the real-time, and even single-shot measurement, this mid-IR imaging is not a real-time imaging system yet, due to the complicated optical system and relative poor signal-to-noise ratio. We are improving the data acquisition method and signal-to-noise ratio to speed the data collection rate.

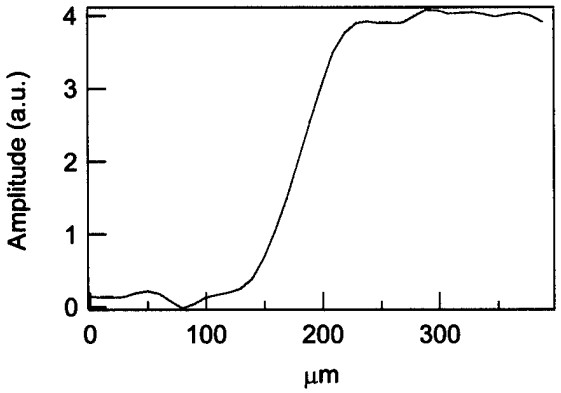

Fig. 5. A razor scans through the THz beam, the derivative of waveform shows a waist of 33 micron.

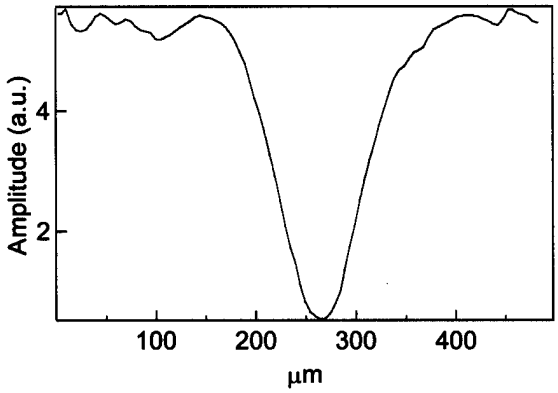

Fig. 6. Scan of an 80-μm human hair.

Figures 5 and 6 plot the transmitted THz field after a razor-blade and a human hair scan through the THz beam focal spot, respectively. It confirms that with the mid-infrared THz pulses, the spatial resolution is less than 40 μm.

(6) Improvement of spatial resolution

To improve spatial resolution of THz imaging, we have concentrated on two tasks. First one is to continuously improve the spatial-temporal resolution (see last month report). We have used a 15 fs laser beam, optimized the imaging system, and we have improved the system's spatial resolution. Figures 7 shows the imaging unit. Figure 8 is the image of three metallic lines (84 μm) on silicon.

ZOmega Technology Corp.
31 Omega Terrace, Latham, NY, 12110
Tel/Fax: (518) 786-1684/6450

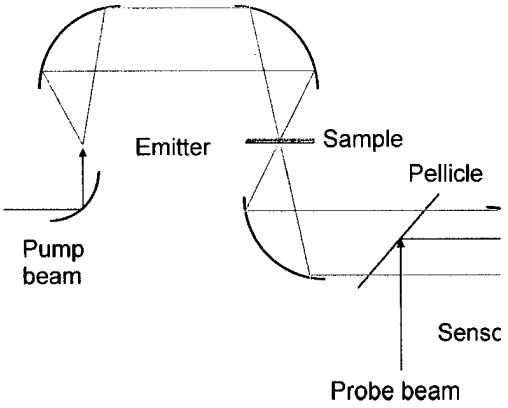

Fig. 7. Mid-IR THz imaging unit. The laser is a 15 fs mode-locked Ti:sapphire laser.

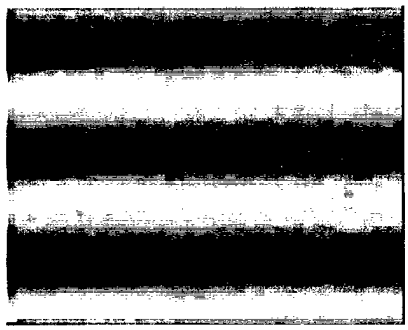

Fig. 8. Transmitted THz imaging of 84-μm metallic transmission lines on a silicon.

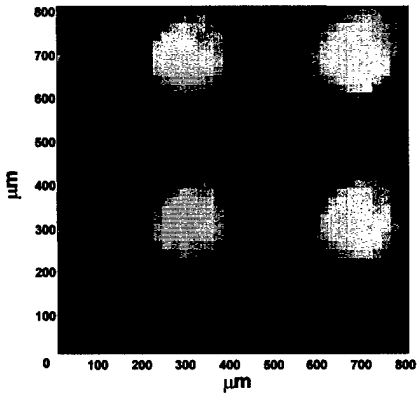

Fig. 9. Transmitted THz imaging of holes (ϕ=100 μm) on a metal plate.

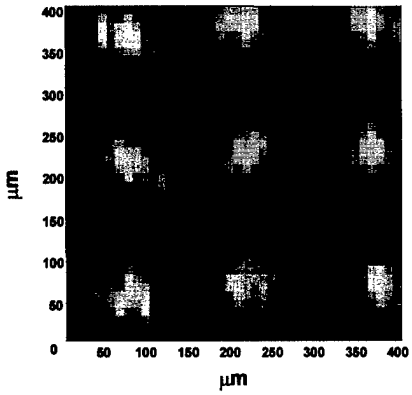

Fig. 10. Transmitted THz imaging of holes (ϕ=50 μm) on a metal plate.

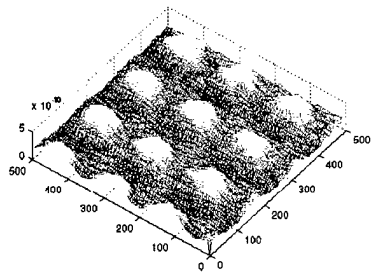

Fig. 11. Transmitted THz imaging of holes (ϕ=25 μm) on a metal plate.

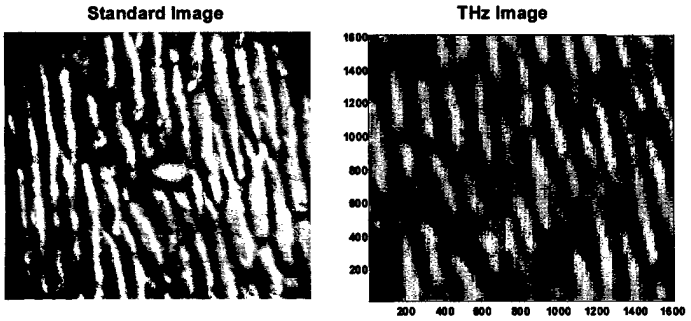

Fig. 12 (a): Microscopy optical image of onion cells; (b) THz images of the same onion skin (1.6x1.6 mm^2). The hole in the image is a postion marker.

Figures 9 to 11 show transmitted THz images from hole arrays on the metal plates. The diameters of the holes are 25 μm, 50 μm, 100 μm, respectively. Figure 12(a) and 12(b)

show the standard optical imaging and THz imaging of a onion skin. These sub-millimeter cells, filled mainly with water, provides us an excellent biological sample for a high resolution THz imaging. The total area of the image is 1.6x1.6 mm^2. The THz image is an E field amplitude image.

(7) An Apparatus for Adjustable Chirp Pulse Measurement

We invented an optical device which can chirp a laser pulse continuously by moving a translation stage. The output direction and timing of the laser beam do not change during the adjustment of the optical pulse duration and the chirping rate. This is a crucial unit in the high-speed THz imaging.

In the chirped pulse measurement, the probe beam is spectrally chirped and temporally stretched by a pair of gratings. It is highly desirable that the chirping rate and the chirped pulse duration is adjustable, but the direction and timing of the laser pulse remains unchanged. We have designed an apparatus to satisfy with such requirements. This device improves the performance of our previous chirped pulse method by simplifying the optical alignment procedure and keeping the same timing during the measurement.

There are two basic requirements for this setup

1. The direction of the output beam is fixed while adjusting the chirping rate;
2. The total beam path is fixed so the timing is unchanged.

Once these two requirements are met, there is not necessary to re-adjust the probe beam (requirement 1) and not necessary to re-find the time zero (requirement 2).

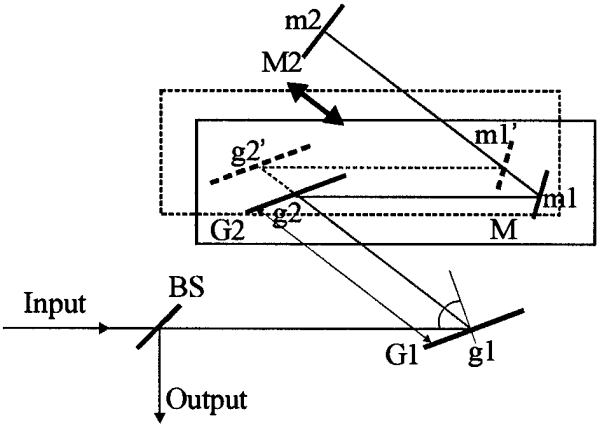

Fig. 13. Schematic of the device with adjustable chirping rate.

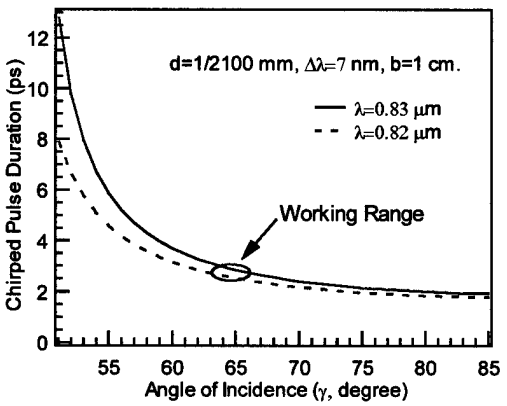

Fig. 14. Chirped Pulse Duration versus the Angle of Incidence relation for 1 cm slant distance b. The parameters are shown in the figure. The ellipsoid shows the working range in the real experiment.

Figure 13 shows the schematic of the setup. G1, G2: optical gratings; M1, M2: optical mirrors; BS: beam splitter. Both G2 and M1 are fixed on a translation stage (square box in the figure), the thick double-end arrows represent the moving axis of the stage. When

the stage is moved, the new positions are denoted by dashed ones, and with prime next to the letters. In the figure, b is the slant distance between grating G1 and G2, γ is the incident angle. To realize the above performances, it is required that

1. $\overline{m1m2}$ must be in parallel with $\overline{g1g2}$;
2. G2 and M1 are on the same translation stage (the blue box); and the moving axis of the stage must be in parallel with $\overline{g1g2}$, $\overline{m1m2}$;
3. Mirror M2 is perpendicular to $\overline{m1m2}$.

When the dashed box is moved by moving the translation stage, G2 and M1 at g2 and m1 are moved to the new positions g2' and m1' (dashed beam paths shown in the Fig. 13). ① Because the moving axis of the dashed box is in parallel with $\overline{g1g2}$ or $\overline{m1m2}$, and the beam is reflected back along the incoming beam path, so the direction of the output beam is unchanged during the movement. ② It is easily seen that $\overline{g2'm1'} = \overline{g2m1}$ and $\overline{g2g2'} = \overline{m1m1'}$, therefore the total beam path or the timing is unchanged.

After the device, the laser pulse is stretched, the pulse duration is roughly in the measurable time window. When a pair of gratings are used to chirp the laser pulse, the pulse duration ΔT_c after the grating pair is given by

$$\Delta T_c = \frac{b(\lambda/d)\Delta\lambda}{cd\left[1-(\lambda/d-\sin\gamma)^2\right]} \tag{1}$$

where λ is the central wavelength, $\Delta\lambda$ the spectral width, c the speed of light in vacuum, d^{-1} the groove density of the grating, γ the incident angle and b the slant distance between gratings. (see Fig. 13 for the definitions of γ and b). It is seen that for given gratings and laser pulse, the chirped pulse duration is only determined by the slant distance b and the incident angle γ. Furthermore, when the incident angle is fixed, then the chirped pulse duration is proportional to the slant distance b. Therefore the pulse duration can be easily adjusted by changing the slant distance b.

In our experiment, we have $d = 1/2100\,\text{mm}$, $\lambda \approx 0.83\mu\text{m}$ $\Delta\lambda = 7\,\text{nm}$. We plot the Chirped Pulse Duration versus the Angle of Incidence for $b = 1$ cm in Figure 14. The ellipsoid shows the working range of this device in the real experiment. Therefore we have roughly 3 ps/cm. Note that this value can be changed by changing the incident angle and the wavelength. Other parameters (such as the grating groove density and the spectral width) are pretty much fixed. With $b = 6\,\text{cm}$, we have $\Delta T_c = 18\,\text{ps}$.

Figure 15 is the simulated chirped pulses in time domain with 2 slant separations of the gratings, assuming Gaussian temporal pulse shape. The pulse duration is proportional to the slant distance b (see Equation (1)). With approximate 3 ps/cm broadening, we have 15 and 30 ps Full Width at Half Maximum (FWHM). The centers of the pulses are at the same time position as required by the design.

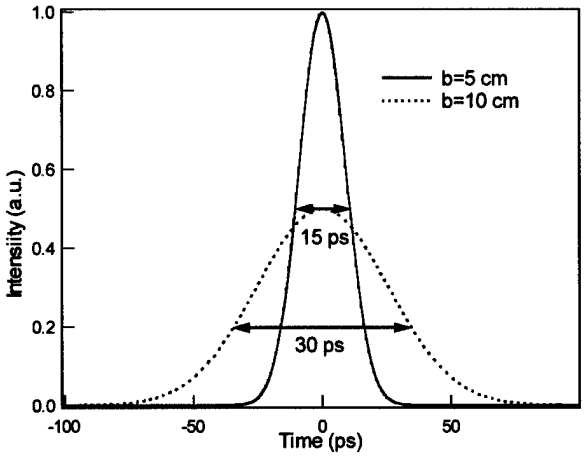

Fig. 15. Simulated chirped pulses in time domain with two slant distances $b = 5$ and 10 cm. The pulse widths of the full width at half maximum are 15 ps and 30 ps, respectively.

(8) Real-time and single-shot THz imaging

Theoretical Analysis

The measuring principle can be understood according to Figure 16. A femtosecond laser beam is split into pump and probe beams. The geometry is similar to the conventional free-space electro-optic sampling setup, except for the use of a grating pair for chirping and stretching the optical probe beam, and a grating-lens combination with a detector array for the measurement of the spectral distribution. Due to the negative chirp of the grating (pulse with decreasing frequency versus time), the blue component of the pulse leads the red component. The fixed delay-line is only used for the positioning of the THz pulse, within the duration of the synchronized probe pulse, (acquisition window) and for temporal calibration.

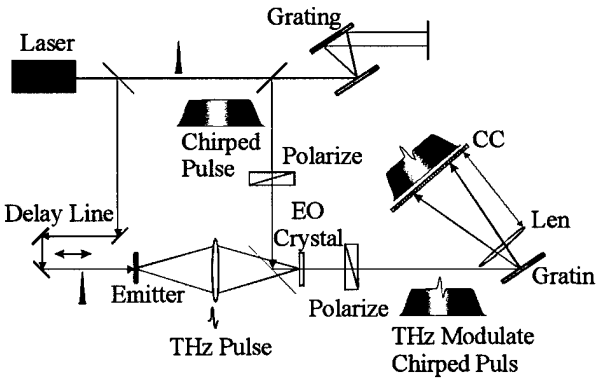

Fig. 16. Schematic of experimental setup of electro-optic measurement with a chirped optical probe beam.

The pump beam is used to generate a THz beam from an emitter, then focused onto the electro-optic sensor via a polythelene lens. The probe beam is frequency chirped and temporally stretched by a grating pair. When the chirped probe beam and a THz pulse co-propagate in the electro-optic crystal, different portions of the THz pulse, through the Pockels effect, modulate the different wavelength components of the chirped pulse. Therefore, the THz waveform is encoded onto the wavelength spectrum of the probe beam. A spectrometer and a detector array (LDA or CCD) are used to measure the

spectral distribution. The temporal THz signal can be extracted by measuring the difference between the spectral distributions of the probe pulse with and without THz pulse modulation.

We can also prove mathematically that the measured signal is proportional to THz field under some conditions. Assuming that the unchirped probe be is a diffraction limited Gaussian pulse with a central frequency ω_0 and an envelope Gaussian function:

$$f_0(t) = \exp\left(-\frac{t^2}{T_0^2} - i\omega_0 t\right), \tag{2}$$

where T_0 is the pulse duration, which is related to the laser spectral bandwidth $\Delta\omega_0$ through $T_0 = 2/\Delta\omega_0$. After diffraction by the grating pair, the electric field component of the chirped probe beam can be written in the form:

$$f_c(t) = \exp\left(-\frac{t^2}{T_c^2} - i\alpha t^2 - i\omega_0 t\right) \tag{3}$$

with 2α is the chirp rate, T_c, ω_0 are the pulse duration and center frequency, respectively. When the chirped probe pulse co-propagates through the EO crystal with a THz field of electric field $E(t-\tau)$, the transmitted probe pulse is given by

$$f_m(t) = f_c(t)[1 + kE(t-\tau)] \tag{4}$$

where τ is the time delay between THz and the probe pulse, and $|k| << 1$ is a constant, the value of k, which is related to the modulation depth, depends on many factors, such as the electro-optic coefficient, optical bias, scattering, thickness of the crystal, and the group velocity mismatch.

Since a spectrometer is used to disperse the probe beam, the spectral modulation is spatially separated on the CCD array. In that case, the measured signal on a CCD pixel with optical frequency ω_1, is proportional to the convolution of the spectral function of the spectrometer and the square of the Fourier transform of the chirped pulse:

$$M(\omega_1) \propto \int_{-\infty}^{+\infty} g(\omega_1 - \omega)\left|\int_{-\infty}^{+\infty} f_m(t)\exp(i\omega t)dt\right|^2 d\omega, \tag{5}$$

where $g(\omega_1 - \omega)$ is the spectral function of the spectrometer. By using Equation (4), Equation (4) can be written as:

$$M(\omega_1) \propto \int_{-\infty}^{+\infty} g(\omega_1 - \omega) \times \left|\int_{-\infty}^{+\infty} \exp\left(-\frac{t^2}{T_c^2} - i\alpha t^2 - i(\omega_0 - \omega)t\right)[1 + kE(t-\tau)]dt\right|^2 d\omega, \tag{6}$$

The integral in Equation (6) can be evaluated by using the method of stationary phase if α is sufficiently large. Since T_c and the THz pulse duration are much longer than the oscillation period of the optical beam ($2\pi/\omega_0$), the factor $\exp\left(-t^2/T_c^2\right)[1+kE(t-\tau)]$ is a slowly varying function of time. The phase factor in Equation (6) gives a self-canceling oscillation, so as to allow the contribution of the integrand to be neglected everywhere except in the vicinity of certain critical points. At the critical point the derivation of the Equation (6) with respect to t is zero. In this case it gives:

$$t_\omega = \frac{\omega_0 - \omega}{2\alpha}. \tag{7}$$

Defining a normalized differential intensity:

$$N(\omega_1) = \frac{M(\omega_1)\big|_{\text{THz on}} - M(\omega_1)\big|_{\text{THz off}}}{M(\omega_1)\big|_{\text{THz off}}}, \tag{8}$$

it can be proved that $N(\omega_1)$ is proportional to the input THz field under certain approximations. Since $|k| << 1$ is true for typical electro-optic measurements, by taking the first order of k, and applying Equation (8), we have:

$$N(\omega_1) = \frac{\int_{-\infty}^{+\infty} g(\omega_1-\omega)2kE(t_\omega-\tau)\exp\left(-2t_\omega^2/T_c^2\right)\mathrm{d}\omega}{\int_{-\infty}^{+\infty} g(\omega_1-\omega)\exp\left(-2t_\omega^2/T_c^2\right)\mathrm{d}\omega}. \tag{9}$$

When the spectral resolution is so high that the spectral function of spectrometer can be expressed as a δ function, we will have

$$N(\omega_1) \propto 2kE(t_{\omega_1}-\tau). \tag{10}$$

This equation shows that the measured spectral profile is indeed proportional to the temporal profile with respect to the input of the THz waveform when the chirp rate is sufficiently large and the resolution of the spectrometer is sufficiently high. The validity and the influence of these conditions will be discussed in the following sections.

Experimental Setup

The laser is an amplified Ti:sapphire laser (Coherent Rega 9000) with an average power of 0.9 W and a pulse duration of 200 fs at 250 kHz. The center wavelength of the Ti:sapphire lasers is about 820 nm with a spectrum bandwidth of 7 nm. The THz emitter is an 8-mm wide GaAs photoconductor with the bias voltage ranging from 2 kV to 5 kV. The focal lens for THz beam is a polythelene lens with 5 cm focal length. 4 mm thick <110> ZnTe crystal is used. The optical probe pulse is frequency chirped and time stretched by a grating pair, and the time window can be easily changed by changing the grating distance. This distance is several centimeters corresponding to the time window

of tens of picoseconds. For electro-optic modulation, two polarizers are used with perpendicular polarization in order to get the highest modulation depth induced by THz field. The dispersion element is a spectrometer (Instrument SA, SPEX 500M) with spectral resolution of 0.05 nm, and dispersion of 1.6 mm/nm. The detector array is a CCD camera (Princeton Instruments, Inc., CCD-1242E). This CCD camera has 1152x1242 pixels and a full well capacity greater than 500,000 electrons, dynamic range 18 bits, and minimum exposure time 5 ms. The data are transferred to a PC computer.

Experimental Results

The experimental resulted will be presented for three cases: single point measurement, spatio-temporal imaging and dynamic subtraction.

1. Single point measurement

In this case, the chirped probe beam is focused onto the EO crystal, and hence THz waveform of a single point is measured. Figure 17 shows the spectral distributions of the chirped probe pulse with and without THz modulation and the differential spectrum distribution (ΔI). This differential distribution reconstructs both the amplitude and phase of the temporal waveform of the THz pulse. The differential spectrum (ΔI) in Figure 17 shifts horizontally by adjusting the fixed delay line. Moving the fixed delay line is equivalent to placing the terahertz field in a different portion of the probe beam spectrum and it can be used as a marker to calibrate the time scale.

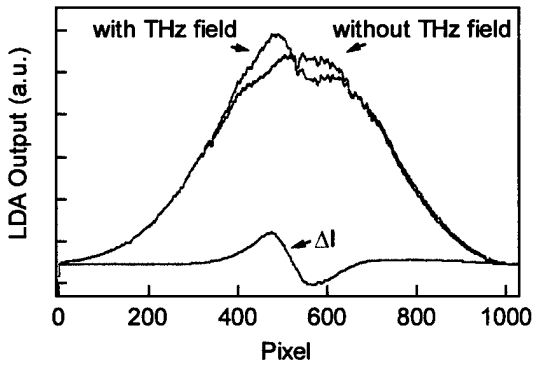

Fig. 17. Spectral distribution of the chirped probe pulse with & without a co-propagating THz field pulse.

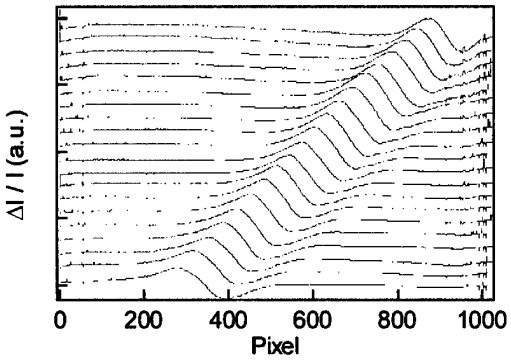

Fig. 18. Normalized differential spectral distribution (ΔI/I) by adjusting the fixed delay line at a step of 1.3 ps.

Figure 18 shows the normalized differential spectrum distribution (ΔI/I) when adjusting the fixed time delay line at a step of 1.3 ps. The offset of the spectrum is shifted for better display. The noise at the edge pixels comes from the spectrum normalization with a small background. These waveforms shift linearly with the fixed time delay step. The total spectral window (1024 pixels) is equivalent to 44 ps, corresponding to 43 fs/pixel.

The results shown in Figure 17 and 18 are obtained with a single CCD exposure, but with thousands of laser pulses. However unlike the conventional sampling techniques, where

The results shown in Figure 17 and 18 are obtained with a single CCD exposure, but with thousands of laser pulses. However unlike the conventional sampling techniques, where only a small portion of the entire THz waveform is measured at each time, for this chirped pulse measurement technique each pulse contains all the information of the entire THz pulse, therefore the single-shot measurement is possible. Figure 19 gives the first *single-shot* measurement of a THz pulse, the signal-to-noise ratio (SNR) is better than 60:1. In this experiment, we took a single-shot spectrum without the THz field first and saved it as the background, then we took a single-shot spectrum with the THz field and performed a subtraction of the background. Although this is not real single-shot in the sense that we need to take the reference spectrum, the real single-shot experiment can be done with dynamic subtraction, which will be given in the part 3 of this section.

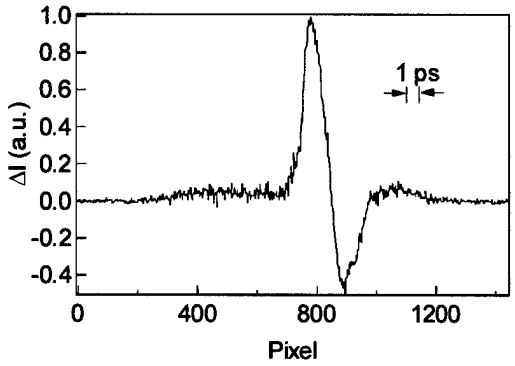

Fig. 19. A *single-shot* spectral waveform of a THz pulse measured by a chirped optical probe pulse. It reconstructs the temporal waveform of the THz pulse.

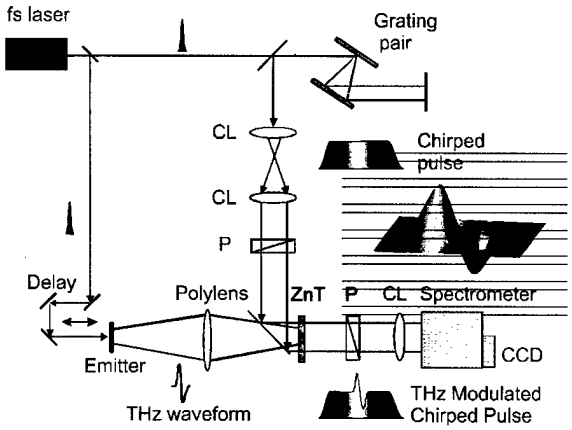

Fig. 20. Schematic of experimental setup for spatio-temporal THz Imaging. Unlike in Fig. 1, cylindrical lenses (CL) are used to focus the probe beam to a line on ZnTe crystal and then image it to the entrance plane of the spectrometer.

2. Spatio-temporal imaging

With slight modification of Figure 16, it is possible to get 1D spatial information of THz field. As shown in Figure 20, the probe beam is focused to a line onto the EO crystal by cylindrical lens, the imaging of this line is formed at the entrance plane of the spectrometer, therefore 1D spatial and 1D temporal information of the THz field is measured simultaneously.

The experimental procedure is the same as for single point measurement, that is the background spectrum is taken and saved as the reference with THz off, and then the another spectrum is measured with THz on, the difference gives the signal. Figures 21 and 22 show the measured distribution images of THz fields (x position versus time) emitted from dipole and quadrupole emitters, respectively. The measured spatial resolution in the imaging system is better that 1 mm, which is close to diffraction limited resolution in other unchirped THz techniques.

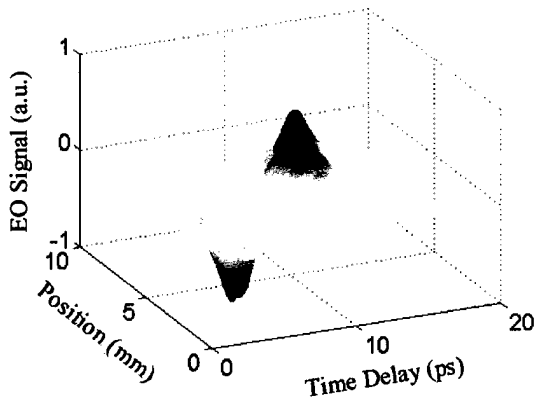

Fig. 21. 1-D THz imaging of a dipole.

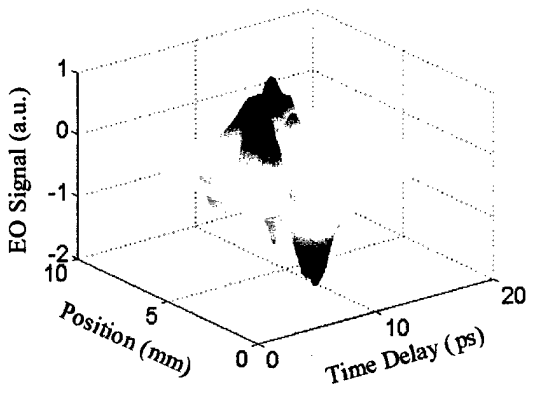

Fig. 22. 1-D THz imaging of a quadrupole.

Figure 23 is a plot of a *single-shot* image from a GaAs photoconductive dipole antenna. This plot contains original data without the signal average and smoothing. The total time for wavelength division multiplexing and demultiplexing is within a few picoseconds. The dipole length is 7 mm, and the bias voltage is 5kV. One-dimensional spatial distribution across the dipole and its temporal THz waveform are obtained simultaneously in a single laser pulse. The size of the spatio-temporal image is 10 mm by 25 ps. In this single-shot measurement the background light per pixel on the CCD camera is ~ 200 counts, whereas that of the modulated probe pulse is ~ 50. Typical oscillation features and the symmetric spatial distribution of the far-field pattern from a dipole photoconductive emitter are obtained.

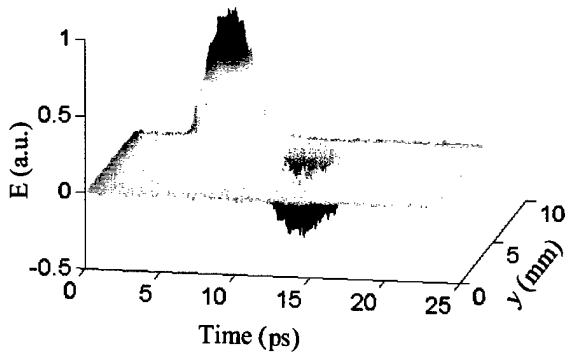

Fig. 23. Single-shot 1-D THz imaging of a dipole field without any signal average. The y-axis corresponds to the spatial position across the dipole emitter.

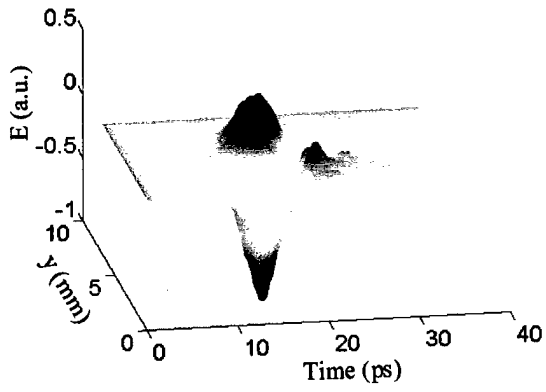

Fig. 24. 1-D THz imaging of a quadrupole field. The y-axis corresponds to the spatial position across the quadrupole emitter.

Figure 24 shows a spatio-temporal image of the THz field from a quadrupole antenna. The size of the spatio-temporal image is 10 mm by 40 ps. The quadrupole has three parallel electrodes separated by 3 mm. The center electrode was biased and the two adjacent electrodes were grounded. The field pattern from two back-to-back dipoles shows opposite polarity depending on the spatial position (y axis). Temporal oscillation from each dipole can be resolved individually. The layered structure in the y-axis direction is due to the optical inhomogeneity of the sensor crystal. A defect point in the ZnTe crystal causes an offset in the field strength of the temporal waveform (E axis in the figure). A high-quality ZnTe crystal with good spatial homogeneity will provide better spatial resolution.

3. Real single-shot measurement (dynamic subtraction)

As mentioned before, to get THz signal, we need two CCD exposures, one without THz modulation and one with THz modulation, therefore they are not real single-shot measurement. However, since a 2D CCD camera is used, it is very easy to measure the spectra without and with THz modulation at the same time using different CCD location. Figure 25 shows the setup. Before the second polarizer, a beam splitter is used to pick up part of the beam, this beam is used as a real-time reference (R) and sent to the spectrometer with the signal beam (S) simultaneously.

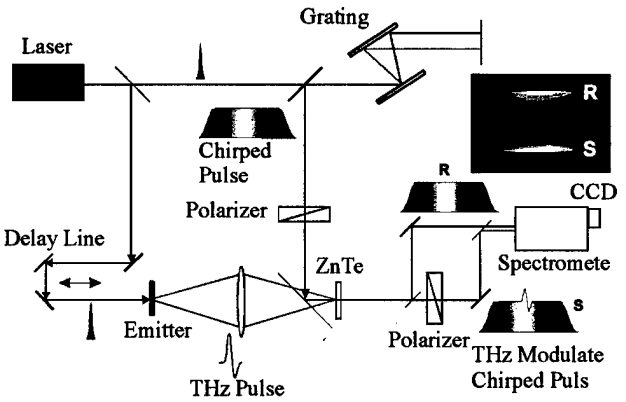

Fig. 25. Dynamic subtraction. The signal beam (S) and the reference beam (R) are sent to the spectrometer simultaneously. Because the reference beam is picked up before the second polarizer, the THz modulation is negligible and can be used as a good reference.

This dynamic subtraction, on one hand, realizes real single-shot measurement, and improve the signal-to-noise ratio on the other hand because the signal spectrum and the reference spectrum are from the same laser pulse, therefore the laser fluctuation is mostly canceled. Figure 26 is the single-shot experimental results. The left panel is the images of the CCD spectral traces of the signal (S) and reference (R) beam, the right panel is the plots of these spectra. When there is no THz, the signal and the reference spectra have good overlap, indicating that the reference is good. When THz is on, its modulation on the signal spectrum is obviously visible even in the CCD image picture. The right panel is the spectra for the reference and signal beams. Again, the differential spectrum gives THz waveform.

This dynamic subtraction is demonstrated only for the measurements of a single spatial point, it is also possible for the spatio-temporal imaging, because only part of the CCD is used in the above imaging. However it is more difficult to align the optics, and needs

more work to do data processing, including pattern match and the correction of the inhomogeneity of the EO crystal.

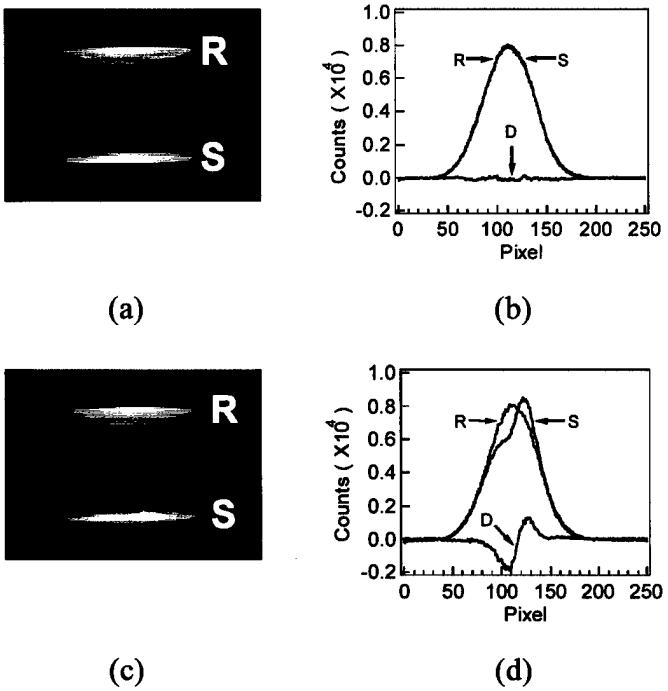

Fig. 26. Results of the dynamic subtraction. The left panel is the images of the CCD spectral traces without THz signal (a) and with THz signal (c). The right panel is the spectral plots without THz signal (b) and with THz signal (d). The difference spectra are also plotted. Notions: R: reference, S: signal, and D: difference.

Improvement

Dynamic Subtraction. The major noise of the THz imaging comes from the laser intensity fluctuation, both spatially and temporally. In the conventional EO sampling, the spatial fluctuation does not contribute to the noise because the whole probe beam is focused onto the detectors. However, with a CCD camera, the spatial fluctuation does contribute to the noise. It can only be corrected if an identical reference picture of the same probe laser beam is taken. We have studied the capability of using a reference image to suppress the spatial and temporal fluctuation. Fig.27 is the setup schematic. The image is split into two identical images by a Wollaston prism. The results are shown in Fig. 28. The corrected picture (c) is more uniform than the un-corrected (b).

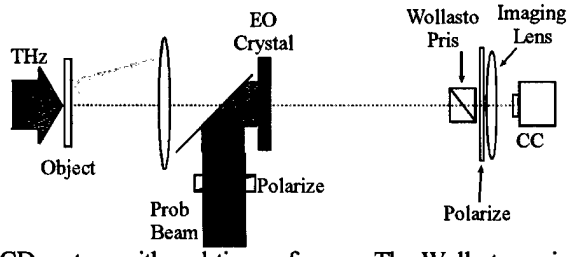

Fig. 27. Schematic of the CCD system with real-time reference. The Wollaston prism splits the probe beam into two beams. These two beams are identical except the intensities.

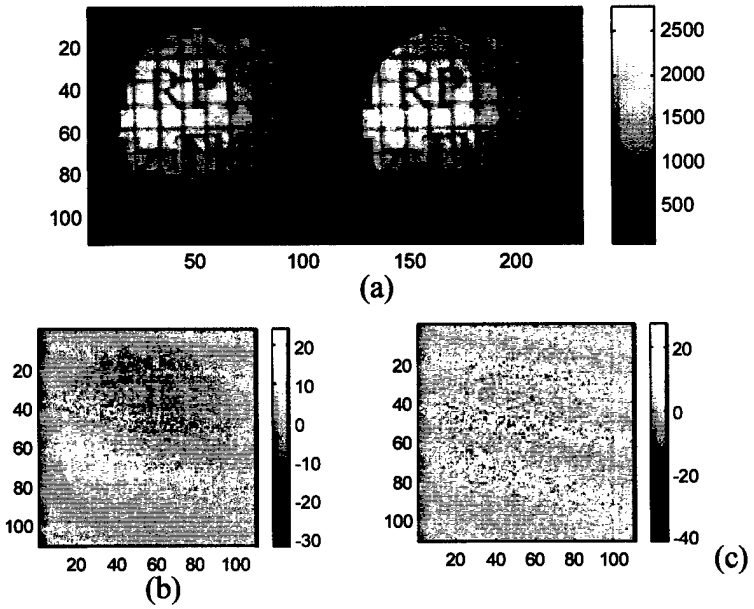

Fig. 28. Suppression of the laser fluctuation by real-time reference. Two identical images are split by a Wollaston prism (a). Noise picture without (b) and with (c) real-time reference.

Software Lock-in CCD. The CCD can be operated in the "lock-in" fashion, i.e., it is synchronized to the chopper. The signal image is obtained by subtracting the image without THz modulation from the image with THz modulation. The SNR is improved by averaging. Fig. 10 plots the spatio-temporal imaging of an optical rectification emitter obtained in the dynamic subtraction with a CCD, which has a 26 Hz frame rate. The SNR is greatly enhanced. Due to the 1/f property, it is highly desired to use a high frame-rate CCD. However, a CCD with 2 kHz frame rate and greater than 12 bits dynamic range is not available.

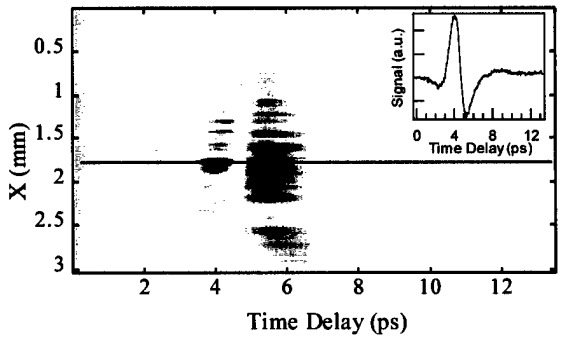

Fig. 29. Spatio-temporal THz imaging of an optical rectification emitter taken with CCD operating in the "lock-in" mode. The horizontal lines come from the inhomogeneity of the EO crystal. The inset is the waveform along the solid horizontal line.

Hardware Lock-in CCD. The conventional lock-in amplifier is obviously not applicable to the CCD detection, and this is the main reason for the low SNR in the CCD system. Fortunately, the so-called lock-in CCD is emerging. This lock-in CCD is originally designed for laser ranging, not optimized for the lock-in detection, but it can, in principle, be used for our purpose. We have one of the lock-in CCD chip, and are going to test it in our CCD imaging system. The appearance of this lock-in CCD will greatly enhance the performance of our CCD system, the optics community at large may benefit too.
Assuming we have a lock-in CCD, and the ability of suppressing noise is as good as that of the lock-in amplifier, then the CCD system will have about the same SNR. The

reasoning is: assuming there are $N \times N$ pixels, due to the parallel measurement property, the integral time for each pixel is $N \times N$ times the integral time used in the scanning system. Hence the noise is only $1/N$. However, as discussed before, the THz beam must be expanded to cover the whole object. Under the diffraction limit, the THz electric field is $1/N$ too. Therefore the overall SNR is comparable. Under these conditions, the CCD system has two advantages: (1) because there is no mechanic scanning, the effective integral time can be longer; (2) if a very powerful THz source is used, and the SNR is unnecessarily high, then the integral time can be decreased to boost the frame rate.

(9) A commercial THz unit

After we achieved the goal of STTR Phase I, we would like to construct a prototype that allows two-dimensional imaging of THz waves with a spatial resolution of better than 100x100 pixels at video frame rates. To do this we plan to start it from a portable THz system. We have ordered and received most of optical components for the construction of the 4th generation of the THz system. For the portability, we plan to use a fiber laser from IMRA (OEM price is $60,000, but we expect the price will drop significantly within two years). The estimated time for packaging and assembling of this portable THz unit is 3 to 5 months, and we hope we can demonstrate this unit in the short course Prof. Zhang will teach, "Free-Space THz Optoelectronics," in CLEO'99, Baltimore.

A list of the optical components required for the assembling a THz system has been competed. The revised design of the portable THz sensor unit (the 4th version of design blueprint) has been finished. The designed THz sensor system has:

THz peak power:	1 mW (with IMRA fiber laser)
Power sensitivity:	< 0.01 mW
Maximum scan length:	70 ps
Spectral range:	33-50 cm^-1 (1 - 1.5 THz)
Size:	12.7"(L)x12.7"(W)x7.4"(H)
Weight:	4 kg, or 8 kg with the IMRA laser

We started to evaluate a fiber laser (FemtoLite-15, IMRA) as a possible candidate for optical source in the portable THz sensor system. This laser is the first commercially available femtosecond fiber laser from IMRA America, Inc. The laser has an average power of 15 mW, pulse duration of 150 fs, wavelength at 780 nm, and a laser repetition rate of 50 MHz. The previous research indicated over 5,000:1 signal-to-noise ratio once this fiber laser was used. The gas spectroscopy (absorption in THz range) of methanol and acetone were obtained with the use of the fiber laser. Rensselaer Machine Shop and a local company in Troy, NY could provide all machine work during the assembling process.

Rensselaer team also study new emitters and sensors for the portable THz sensor system. They observed strong THz radiation in Mid-Infrared range (10 to 15 THz) once a DAST crystal was used as an electro-optic emitter. The radiated field strength from a DAST

crystal is at least twice stronger than the use of a ZnTe, which is the best crystal known in this wavelength.

(10) Publications and patent partially supported by this STTR Phase I.

1. Physics Update, Physics Today, page 9, August, 1998.
2. Zhiping Jiang, F.G. Sun, X.-C. Zhang, "Spatio-temporal Imaging of THz Pulses," 1998 IEEE Sixth International conference on Terahertz Electronics Proceedings, P.94-97, edited by P. Harrison. IEEE Catalog Number: 98EX171. Weetwood Hall, The University of Leeds, 3rd and 4th September 1998.
3. X.-C. Zhang and Zhiping Jiang, "Imaging of Far-Infrared THz Pulses," in Hot Topic, LEOS Newsletter, Vol. 12, No. 6, 7 (1998).
4. Zhiping Jiang, F.G. Sun, Q. Chen, X.-C. Zhang, "Electro-Optic Sampling near Zero Optical Bias Point," Appl. Phys. Lett. 74, 1191-1193 (1999).
5. Zhiping Jiang, X.-C. Zhang, "Chirped Pulse Measurement Techniques of THz Spatio-Temporal Distribution," to be published in IEEE Transactions on Microwave Theory and Techniques. (invited)
6. Zhiping Jiang and X.-C. Zhang, "THz Imaging via Electro-Optic Effect," Invited Talk. 1999 IEEE MTT-S International Microwave Symposium(IMS).
7. Zhiping Jiang, F. G. Sun, Q. Chen, and X.-C. Zhang, "Electro-Optic Sampling near Zero Optical Transmission Point," CLEO'99
8. Q. Chen, Zhiping Jiang, F. G. Sun, and X.-C. Zhang, "Two-Fold Improvement of THz Optoelectronic Generation and Detection," CLEO'99
9. Q. Chen, Zhiping Jiang, and X.-C. Zhang, "All-optical THz Imaging," (invited paper), Terahertz Spectroscopy and Applications, SPIE's Photonics West '99, San Jose, Jan. 1999. (Vol. 3617-14)
10. X.-C. Zhang, Zhiping Jiang, and M. Litz, "Imaging THz Fields by Using a Chirped Optical Beams," The Ninth Annual DARPA Symposium on Photonic Systems for Antenna Application. Monterey, California, February 1999.
11. Zhiping Jiang and X.-C. Zhang, "Chirped Pulse Measurement Techniques of THz Spatio-Temporal Distribution," Journal of High Speed Electronics, submitted (1999).
12. X.-C. Zhang and Zhiping Jiang, "Electro-Optic Measurement of Terahertz Field Pulse with Chirped Pulse," filed for U.S. patent application, January 29, (1999).

There are about 100 groups worldwide working on THz programs or THz related projects. We have established a communication network with these people. We contacted and collaborated scientists and representatives from industrial companies on commercialization of the THz sensors and THz imaging systems. For example, we work closely with Dr. O'Conner's group, Boston Medical Center on THz imaging in breast cancer application.